A tissue-level electromechanical model of the left ventricle: Application to the analysis of intraventricular pressure.

Virginie Le Rolle [1, 2], Guy Carrault[1, 2], Pierre-Yves Richard [3], Philippe Pibarot[4], Louis-Gilles Durand[5], Alfredo I. Hernández [1, 2]

1 INSERM, U642, Rennes, F-35000, France;

2 Université de Rennes 1, LTSI, Rennes, F-35000, France;

3 Supelec IETR, avenue de la Boulaie, B.P. 81127, 35511 Cesson-Sévigné cedex, France

4 Institut de cardiologie de Québec, Hôpital Laval, Université Laval, Ste-Foy, Québec, Canada

5 Institut de recherches cliniques de Montréal, Université de Montréal, Montréal, Québec, Canada, H2W 1R7

Corresponding Author :

Virginie Le Rolle

LTSI, Campus de Beaulieu, Université de Rennes 1, 263 Avenue du General Leclerc - CS 74205- 35042 Rennes Cedex, France.

virginie.lerolle@univ-rennes1.fr

Abstract:

The ventricular pressure profile is characteristic of the cardiac contraction progress and is useful to evaluate the cardiac performance. In this contribution, a tissue-level electromechanical model of the left ventricle is proposed, to assist the interpretation of left ventricular pressure waveforms. The left ventricle has been modeled as an ellipsoid composed of twelve mechano-hydraulic sub-systems. The asynchronous contraction of these twelve myocardial segments has been represented in order to reproduce a realistic pressure profiles. To take into account the different energy domains involved, the tissue-level scale and to facilitate the building of a modular model, multiple formalisms have been used: Bond Graph formalism for the mechano-hydraulic aspects and cellular automata for the electrical activation. An experimental protocol has been defined to acquire ventricular pressure signals from three pigs, with different afterload conditions. Evolutionary Algorithms (EA) have been used to identify the model parameters in order to minimize the error between experimental and simulated ventricular pressure signals. Simulation results show that the model is able to reproduce experimental ventricular pressure. In addition, electro-mechanical activation times have been determined in the identification process. For example, the maximum electrical activation time is reached, respectively, 96.5 ms, 139.3 ms and 131.5 ms for the first, second, and third pigs. These preliminary results are encouraging for the application of the model on non-invasive data like ECG, arterial pressure or myocardial strain.

Keywords:

Biomedical Systems modeling, Biomedical Model Simulation, Model-Based Interpretation, Identification, Ventricular pressure.

Introduction

The evaluation of cardiac performance is one of the most challenging tasks in cardiology. This evaluation is often based on the analysis of blood pressure measurements, which can be performed invasively or non-invasively, in a discrete or continuous manner. Typically, values of diastolic and systolic pressures are acquired and monitored over time, but the information contained in the morphology of pressure signals is generally not exploited. Mathematical modeling of the cardiac mechanical activity can be useful in this sense.

A variety of mathematical models of the ventricular function have already been proposed. The left ventricle can be represented simply by a time-varying elastance (Guarini et al. 1998; Palladino et al. 2002) that can give realistic simulations of global cardiac characteristics. However, since this approach represents the whole left ventricle (LV) with a single element, it is not possible to reproduce ventricular pressure in particular cases, for example, during the electro-mechanical desynchronisation of one part of the myocardium, as observed in some patients suffering from heart failure. Other approaches have been proposed in order to represent explicitly, at different levels of detail, cardiac electrical activity (Luo et al. 1994; ten Tusscher et al. 2004), excitation-contraction coupling (Wong 1973; Hunter 1995; Rice et al. 2000; Kerckhoffs et al. 2003), cardiac mechanical activity (Chaudhry 1996; Nash 1998; Kerckhoffs et al. 2003) and mechano-hydraulic coupling (Verdonck 2002; Kerckhoffs et al. 2007).

Complete models of ventricular activity are developed from a combination of these different energy domain descriptions (Nash 1998; Kerckhoffs, Faris et al. 2003). A fine-grained description of the ventricular activity (at the cellular or sub-cellular levels) is presented in the most detailed approaches. They have been shown to be useful for the analysis of regional myocardial dynamics (Nash 1998; Nickerson et al. 2005) or to study the influence of mechanical stresses on ventricular fibrillation, by integrating specific ionic currents, excitation–contraction coupling, anisotropic nonlinear deformation of the

myocardium, and mechano-electric feedback (Hirabayashi et al. 2008).

However, these approaches require significant computational resources and are characterized by a large number of parameters. These aspects reduce the model identifiability, make it more difficult to couple these models with models of other physiological systems (e.g., circulation), and thus limit their application to our problem. Complete models of the cardiovascular system, that include tissue-level descriptions of the electrical activity of the heart, the electro-mechanical coupling in the ventricles, the circulation and the Autonomic Nervous System (ANS) have already been proposed in other studies (Shim et al. 2008) and in our previous works (Le Rolle et al. 2005; Le Rolle et al. 2008). However, in these models, the asynchronous contraction of the different myocardial walls was not taken into account and it is thus not possible to simulate realistic ventricular pressure morphologies.

As previously stated, the main objective of the present work is to propose a personalized model-based approach to reproduce and interpret left ventricular pressure waveforms. A new model has been developed, with the following specific properties: *i)* the model resolution stands at an intermediate scale, since it takes into account a limited number of coupled tissue-level elements; *ii)* The model is based on functional integration of interacting physiological processes, by taking into account electro-mechanical coupling, the coupling of blood inside the cavity with the myocardial wall, as well as a simplified representation of the systemic circulation.

This allows the representation of the main cardiac properties required to tackle the problem under study, such as the Frank-Starling law and the influence of preload and afterload. The variety of energy domains, the spatial scale retained (tissue-level) and our desire to build a modular model, led us to use the Bond Graph formalism for the mechano-hydraulic aspects and cellular automata for the electrical activation. These two formalisms have already been proposed in the literature and have shown interesting results and low computational costs (Bardou et al. 1996; LeFèvre 1999; Hernandez 2000; Hernandez et al. 2002; Diaz-Zuccarini 2003). An original aspect of this work is thus the

combination of Bond Graphs and Cellular Automata into a multi-formalism model of the left ventricle.

The proposed model is used to reproduce and analyze intra-cardiac pressure signals by adapting the model parameters to experimental data. An experimental protocol has been defined to acquire ventricular pressure signals from three pigs. Model parameters are adjusted to the data by minimizing the difference between real and simulated ventricular pressure signals by using Evolutionary Algorithms (EA).

This paper is organized as follows: in a first section, the proposed model is described in detail before introducing the identification method. Section two presents the experimental protocol employed. Acquired and simulated signals are compared for the different physiological conditions (steady-state, afterload, and ischemia) and identification results are discussed.

Methods

Model description

An ellipsoidal geometry has been chosen to model the left ventricle, as it is close to the real anatomical shape, and yet quite simple. The myocardial wall has been divided into 12 segments (Silva et al. 2002) that are composed of three layers (base, medium and apex). Each layer is separated in 4 components corresponding to the septal, lateral, anterior and inferior walls (Figure 1). Each wall segment interacts with the blood volume inside the intra-ventricular cavity. The shape of the ventricle is defined as an ellipsoid of revolution, which can be described in spherical coordinates by:

$$x = a.\cos\theta.\sin\varphi \qquad\qquad (1)$$

$$y = a.\sin\theta.\sin\varphi$$

$$z = b.\cos\varphi \qquad \text{where } \theta \in [0,2\pi] \text{ and } \varphi \in [0,\pi].$$

Parameters a and b of the ellipsoid are respectively defined as the minor and major ventricular axes.
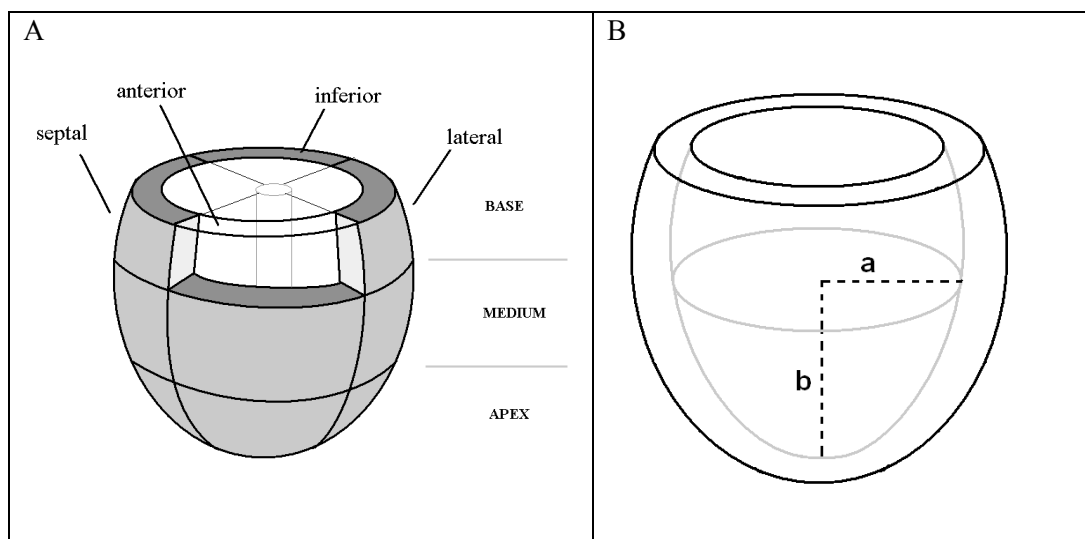
Figure 1 : A) Segmentation of the proposed model of the left ventricle composed of twelve segments at the basal, equatorial and apical level. Each layer is separated into 4 components: septal, lateral, anterior and inferior wall, B) The parameters *a* and *b* of the ellipsoid are respectively defined as the minor and major ventricular axes.

The development of ventricular pressure waveforms during a heart beat is the consequence of the asynchronous electro-mechanical function of the cells associated with each ventricular segment. In order to represent this tissue-level myocardial regional activity, we have chosen to integrate, for each segment, simplified representations of their electrical, electro-mechanical, mechanical and hydraulic activities. The 12 segments are then coupled to the hydraulic and electrical domains to constitute the organ-level model.

Electrical activity

The tissue-level wall segments previously defined contract asynchronously, following the electrical propagation through the ventricular walls. Each myocardial segment has a specific electrical state, which depends on the neighboring segments. The model of the cardiac electrical activity should take into account the propagation of a tissue-level Action Potential (AP) and the electrophysiological status of each segment. The use of a cellular automata network seems to be a judicious choice for this, since it has already given good results concerning electrical cardiac modeling (Bardou, Auger et al. 1996)

and it can reduce simulation time, as the simulation of cellular automata does not require any integration process to compute the change of electrical state.

A four-states cellular automaton is defined for each tissue-level segment (Hernandez 2000; Hernandez, Carrault et al. 2002). The states correspond to specific action potential phases: rapid depolarization period (*RDP*), absolute refractory period (*ARP*), relative refractory period (*RRP*) and waiting period (*idle*). The transitions between states happen at the end of each phase. After the *RDP* period, an automaton transmits a stimulus to its neighboring segments. Each automaton is connected to its three or four neighbors by antegrade, retrograde or lateral connections.

The beginning of the *RDP* corresponds to the beginning of the tissue-level AP, and is called the Electrical Activation Time T_{EA}. At the end of the *RDP*, the *ARP* begins. This instant is defined here as the Mechanical Activation time (T_{MA}). In order to represent, in a simplified manner, the complex processes involved in the electro-mechanical coupling at the tissue-level (e.g. calcium dynamics of each cell composing the tissue, effect of the heterogeneous mechanical activation of each cell, etc.), the choice was made in this work to use an Electro-Mechanical Driving Function (*EMDF*), which is based on a truncated sine function characterized by its amplitude *K* and period *T* (Figure 2) :

$$EMDF = \begin{cases} k_{min} & t_{es} < 0 \\ K\sin(\pi.t_{es}/T_{max}) & 0 \le t_{es} \le T_{max} \\ k_{min} & t_{es} > T_{max} \end{cases} \qquad (2)$$

where t_{es} is the time (ms) elapsed since the T_{MA} for each segment *s*, T_{max} is the activation duration (ms), *K* the maximum value of the *EMDF* signal, which has been defined here to be in a scale similar to the mean tissue-level calcium concentration (μM) and k_{min} is the minimum level of the *EMDF*. In this way, the *EMDF* can be interpreted as the mean calcium concentration level resulting from the set of cells composing a myocardial segment.

Although, this description remains simple, we consider it is accurate enough for this study, as the aim is to investigate the influence of the asynchronous electro-mechanical

function of myocardial segments on ventricular pressure. In this sense, the interpretation of the electromechanical parameters in our model will be limited to the analysis of the relative contribution of each segment to the whole ventricular activity by means of the tuning parameter *T*. It should be noticed that such an analytic approach has been already used in tissue-level models of the whole organ (Bovendeerd et al. 2006), showing a good correspondence with organ and system-level data.
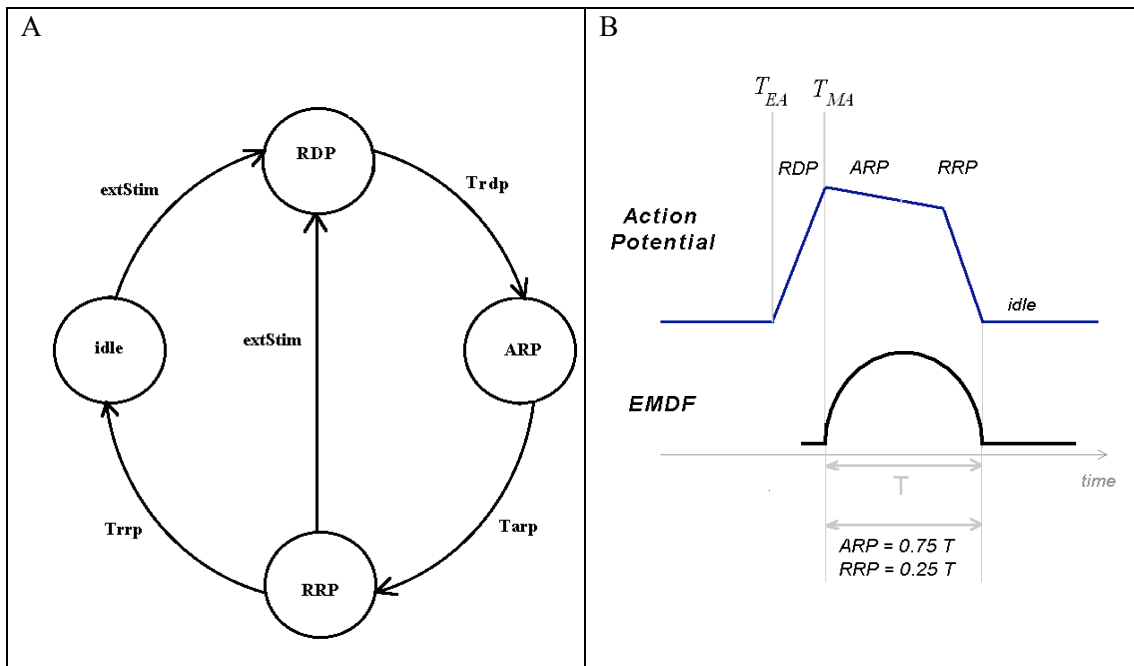

Figure 2 : A) Each automaton is defined by four electrical states: 1. rapid depolarization period (RDP), 2. absolute refractory period (ARP), 3. relative refractory period (RRP) and 4. a waiting period (idle). B) Relation between the automaton states and the electro-mechanical driving function (*EMDF*): T_{EA} and T_{MA} correspond respectively to the electrical activation and mechanical activation instants.

Mechanical activity

Cardiac mechanical properties can be separated into active and passive components. Cardiac tissue deformations are limited by the passive stresses that can be explained by the myocardium organization (fibers, collagen…), whereas actives stresses are generated by the variation of the intracellular calcium concentration. To describe the cardiac mechanical activity, the stress/strain relation must be determined using a constitutive law,

characteristic of the myocardial behavior and the relation between myocardial stress and ventricular pressure must be defined. The whole stress tensor can be expressed as the sum of a passive term and an active term:

$$\sigma = \sigma_{pass} + \sigma_{act} \qquad\qquad (3)$$

Concerning the passive properties, as the material is assumed to be hyperelastic and incompressible, which is a usual assumption for cardiac muscle, the passive stress depends on a strain energy function W:

$$\sigma_{pass} = -pI + 2F\frac{\partial W}{\partial C}F^{T} \qquad\qquad (4)$$

where p stands for the hydrostatic pressure, I is the identity tensor, F the deformation gradient tensor, C is the right Cauchy-Green tensor (Chaudhry 1996; Taber et al. 1996) computed from F : $C = F^{T}F$. Several functions W have been defined in the literature to describe cardiac performance and are based on knowledge of the structure and experimental acquisitions on cardiac tissues. A polynomial energy function (Humphrey et al. 1990) was chosen here because its polynomial form facilitates the implementation and this function has proven useful in many studies (Chaudhry 1996; Taber, Yang et al. 1996):

$$W = c1.(\alpha\text{-}1)^{2}\text{-}c2.(\alpha\text{-}1)^{3}+c3(I1\text{-}3)+c4(I1\text{-}3)(\alpha\text{-}1)+c5(I1\text{-}3)^{2} \qquad \text{with } \alpha = \sqrt{I4}$$

$$(5)$$

where $I1$ and $I4$ stand for the invariants of the deformation gradient tensor. By applying equation (4), the passive stress can be expressed as :

$$\sigma_{pass} = -pI + 2W_{1}B + 2W_{4}FN \times NF^{t} \qquad\qquad (6)$$

$$\text{with } W_{1} = \frac{\partial W}{\partial I1} , \quad W_{4} = \frac{\partial W}{\partial I4} , I1 = tr(C) \text{ and } I4 = N^{t}.C.N$$

where N is a unit vector in the direction of the fiber and ψ is the fiber angle with respect to the parallel direction. Since we know the strain energy function W, the deformation

gradient tensor F should also be defined. In this paper, spherical coordinates are used, and the deformation is assumed to be exclusively radial. Thus, a material particle in the undeformed state (R,Θ,Ψ) goes to (r,θ,φ) in the deformed state, which verifies:

$$r = r(R); \qquad \theta = \Theta ; \qquad \varphi = \Psi \qquad\qquad (7)$$

Then, it is possible to obtain the components of the deformation gradient F in spherical coordinates. Because of the radial motion hypothesis, F becomes a square diagonal matrix the three nonzero elements of which provide the strains λ_r, λ_θ and λ_φ in the principal directions. It can easily be shown that the deformations in the three directions are expressed as: $\lambda_r = \dfrac{\partial r}{\partial R}$ and $\lambda_\theta = \lambda_\varphi = \dfrac{r}{R}$ (common value denoted by λ in the following). As the myocardium has been assumed to be incompressible, it holds: $\det(F) = 1$. So a simple relation between λ_r and λ can be found: $\lambda_r = 1/\lambda^2$ and the invariants are computed as : $I1 = 1/\lambda^4 + 2\lambda^2$ and $I4 = N^t.C.N = \lambda^2$

The other part of the stress tensor due to active properties can be expressed using the relation:

$$\sigma_{act} = T_a.(FN).(FN)^T \qquad\qquad (8)$$

where N still stands for a unit vector in the fiber direction and T_a depends on the intracellular cardiac concentration. The form proposed in (Hunter 1995) is used in this paper and is related to the *EMDF* by the following function:

$$T_a = T_{ref} \frac{EMDF^n}{EMDF^n + Ca_{50}^n}[1 + \beta(\lambda - 1)] \qquad (9)$$

where T_{ref} the value of the tension at $\lambda = 1$, Ca_{50} is the calcium concentration at 50% of the isometric tension, n is the Hill coefficient determining the shape of the curve and β is a nondimensional slope describing the myofilament "cooperativity", which translates the impact of sarcomere length on the level of cardiac activation. The parameters values and functions for Ca_{50} and n are taken from (Hunter 1995). Since the total stress tensor has

been defined as the sum of the active and passive tensors, the three directional components are:

$$\sigma_{rr} = -p + \tilde{\sigma}_{rr} \quad \text{with} \quad \tilde{\sigma}_{rr} = 2.W_1 / \lambda^4 \tag{10}$$

$$\sigma_{\theta\theta} = -p + \tilde{\sigma}_{\theta\theta} \quad \text{with} \quad \tilde{\sigma}_{\theta\theta} = 2.W_1.\lambda^2 + 2.W_4.\lambda^2.\cos(\psi) + T_a.W_4.\lambda^2.\cos(\psi) \tag{11}$$

$$\sigma_{\varphi\varphi} = -p + \tilde{\sigma}_{\varphi\varphi} \quad \text{with} \quad \tilde{\sigma}_{\varphi\varphi} = 2.W_1.\lambda^2 + 2.W_4.\lambda^2.\sin(\psi) + T_a.W_4.\lambda^2.\sin(\psi) \tag{12}$$

This three-equations system is implicit, because it includes four unknown variables σ_{rr}, $\sigma_{\theta\theta}$, $\sigma_{\varphi\varphi}$ and p. The Laplace Relation is added to link the three stress components. This relation has been demonstrated for thin ellipsoidal myocardial segments in (Back 1977), which shows that the thin wall theory is adequate for the estimation of average longitudinal and latitudinal stresses in ventricular walls:

$$p_{fl} = \frac{\sigma_{\theta\theta} \times e}{R_p} + \frac{\sigma_{\varphi\varphi} \times e}{R_m} \tag{13}$$

where R_m and R_p stand for the radii of curvature in the meridian and parallel directions, while e is the wall thickness. Since the ventricle is assumed to be an ellipsoid of revolution, (R_m, R_p) can be expressed as:

$$Rm = \frac{(a^2 \ \cos^2 \varphi + b^2 \ \sin^2 \varphi)^{3/2}}{ab} \quad \text{and} \quad Rp = \frac{a}{b}(a^2 \ \cos^2 \varphi + b^2 \ \sin^2 \varphi)^{1/2} \tag{14}$$

Since the coupling between the fluid and the structure can be locally expressed by the relation $\sigma_{rr} = -p_{fl}$, it is possible to obtain the wall radial force by integrating the radial stress over the segment surface: $F_r = -\int \sigma_{rr} dS$. The explicit expression can be written as:

$$F_r = \tilde{\sigma}_{\theta\theta}.\lambda^2 \ K_\theta + \tilde{\sigma}_{\varphi\varphi}.\lambda^2 \ K_\varphi - \tilde{\sigma}_{rr}.\lambda^2 \ K_r \tag{15}$$

with

$$K_\theta = \iint \frac{1}{1 + \dfrac{R_p}{e} + \dfrac{R_p}{R_m}} .R^2 .\sin\varphi .d\varphi .d\theta$$

$$K_\varphi = \int\int \frac{1}{1 + \dfrac{R_m}{e} + \dfrac{R_m}{R_p}} . R^2 . \sin\varphi . d\varphi . d\theta$$

$$K_r = \int\int \frac{e.R_p + e.R_m}{e.R_m + e.R_p + R_m.R_p} . R^2 . \sin\varphi . d\varphi . d\theta$$

These mechanical relations provide the constitutive law of a capacitive element suitable to model the segment and should be connected with a hydraulic description of the blood in contact with the myocardial wall.

Hydraulic activity

Since the radial force has been computed previously, the ventricular pressure is deduced using the relation:

$$P_{LV} = F_r / S \qquad\qquad (16)$$

where S can be easily calculated since the surface is ellipsoidal: $S = \int\int R^2 . \sin\varphi . d\varphi . d\theta$. Equation (16) expresses the mechanical-hydraulic conversion and can be represented by a Bond Graph element called transformer (see APPENDIX A).

The interaction between the development of force in the deformable structure and the variation of pressure at the surface of the wall has been defined previously. This description must be completed by the representation of the hydraulic behavior of the blood volume in contact with the wall segment to obtain the pressure characteristics from the wall surface (P_S) to the cavity center (P_c). In fact, the fluid mass mainly brings inertial effects that can be defined by the law:

$$P_c - P_s = I \frac{dQ}{dt} \qquad\qquad (17)$$

Moreover, the blood viscosity induces frictions between the fluid and the wall of the vessel. This friction contributes to the resistance to flow, which is defined, in the model, by a hydraulic resistance R. To describe the rapid filling phases, this resistance is considered lower during the diastole (R_{min}) and higher during systole (R_{max}). A resistive law relates pressure and flow:

$$Q = \frac{P_c - P_s}{R} \qquad\qquad (18)$$

Summary of the whole-ventricle model

The myocardial segment and the blood volume in contact with it were modelled first. The electrical activity of each segment is represented by a cellular automaton to give the electrical status and an estimation of the electro-mechanical activation that is associated with the mechanical model. A capacitive Bond Graph element is defined in the mechanical domain since the previously established relations provide a global force that depends on the radius. Next, the energy conversion (equation 16) can be represented by a transformer to connect the mechanical and hydraulic parts. Finally, an inertial effect associated with a resistive effect describes the hydraulic behavior of the fluid, modeling a radial flow (Figure 3.A).
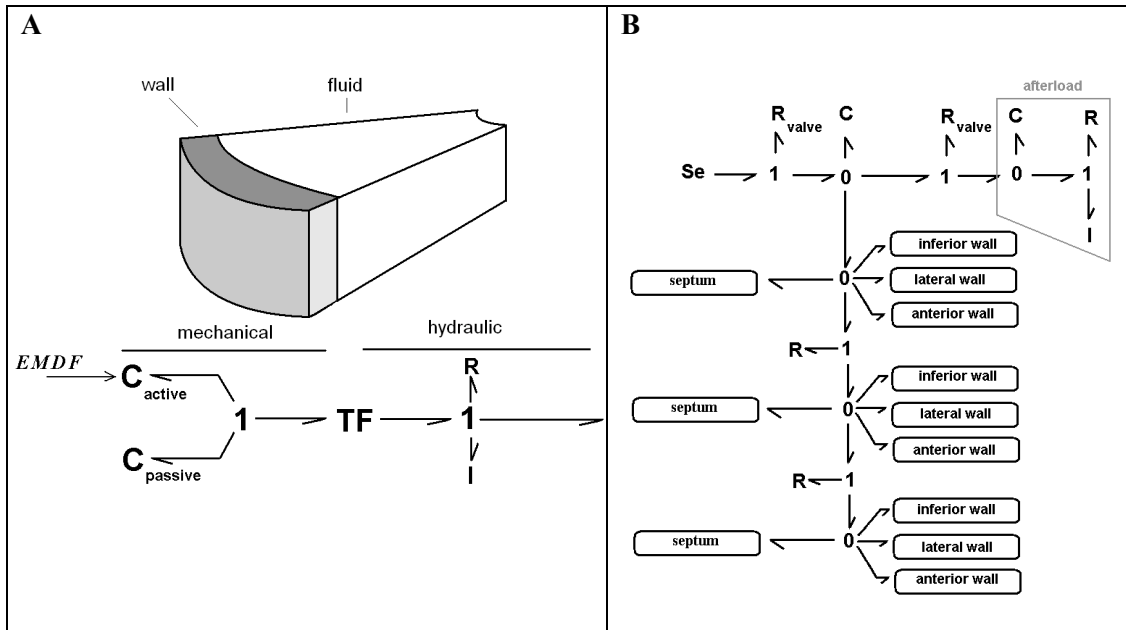
Figure 3: (A) Bond Graph of the segment and the fluid in contact. The *EMDF* is connected to the mechanical model that is composed of two capacitive Bond Graph elements. The energy conversion is represented by a transformer. An inertance and a resistance describe the hydraulic behavior of the fluid. (B) Model of the whole ventricle including the preload (Se), the valves and the afterload (see APPENDIX A). The segments are connected through the hydraulic domain as the pressures are equal and the flow is the sum of each segment's flow.

Connections between segments must also be defined. We represent the ventricle by twelve cellular automata to describe the electrical propagation. An external excitation first stimulates the mid-septum segment. This activation allows the stimulation of the other segments thanks to propagation. In fact, each automaton transmits a stimulation at the end of the *RDP* period. Segments are also coupled through the hydraulic domain (Figure 3.B), since the total flow Q_t is the sum of the regional flows Q_i:

$$Q_t = \sum_i Q_i \tag{19}$$

The connections between the three layers are defined by considering the resistive properties of the blood inside the cavity. These relations are represented in Bond Graph notation by a 0-junction.

The preload has been modeled by a constant effort source. Parallel capacitance, resistance, and inertance describe the aortic obstacle and systemic arteries. The heart valves are represented as non-ideal diodes that correspond to modulated resistances, and the valvular plane is described by a constant capacitance.

The parameters values of afterload (capacitance and inertance) have been taken from the literature (Ursino et al. 2000) and the constant effort source has been deduced from previous simulations to be equal to the venous return flow. The ventricular model includes parameters that describe the mechanical behavior. The values of many of these ($c1$, $c2$, $c3$, $c4$, $c5$, T_{ref}, β, Ca_{50}^n) have been estimated in the literature (Hunter 1995; Chaudhry 1996) (see APPENDIX B). The ellipsoid dimensions correspond to mean values measured on healthy human adults: a = 2 cm et b = 4.8 cm. The myocardial wall is divided into 12 segments. The ventricular length is separated into three parts in order to have equal azimuthal angle. Each layer is divided into four parts, each of which forms an angle of $\pi/2$. It is possible to calculate, on each segment, the surface (S) and the radii of curvature to obtain coefficients K_θ, K_φ, K_r. The other parameters values have to be determined by an identification algorithm, in particular, the mechanical activation period (T_{max}), the maximum activation level (K) and the RDP period. The use of such an identification algorithm relies on the exploitation of experimental data. A protocol has thus been defined to measure the intra-ventricular pressure in pigs.

Experimental Protocol used for the Acquisition of Ventricular Pressure

Experiments were carried out in 2002 at the Laval Hospital Research Center, Laval University, Quebec, on 3 pigs weighing between 36 and 48 Kg. Animal care and experiments were conducted in accordance with the Guidelines of the Canadian Council for Animal Care. The protocol was approved by the Institutional Animal Care Committee of Laval University. The purpose of the experimental studies was to obtain several signals for studying the effects of cardiac inotropy of the left ventricle on acoustical and pressure signals: the electrocardiogram (ECG), the intra-ventricular and the intra-myocardial

pressures, the thoracic, esophageal and epicardial phonocardiograms (PCGs). The recording of the esophageal PCG was done by the insertion of a custom-designed microphone into the esophagus under fluoroscopy guidance until the microphone sensor was located near the inferior base portion of the left ventricle. The thoracic PCG was recorded by placing a microphone on the thorax. In order to measure the epicardial PCG, a left lateral thoracotomy was performed and an accelerometer (Bruel & Kjaer, 4374, 0.65 grams, 1-26000 Hz) was glued to the epicardium of the left ventricular lateral wall close to the apex (Figure 4). The left ventricular pressure was obtained by the insertion of a catheter (Millar Instrument, SPR-350, 5F) through the right carotid artery. The acquisition of the intra-myocardial pressure was performed using a needle-type catheter (Millar Instrument, SPR-477, 2F) inserted inside the myocardial wall.
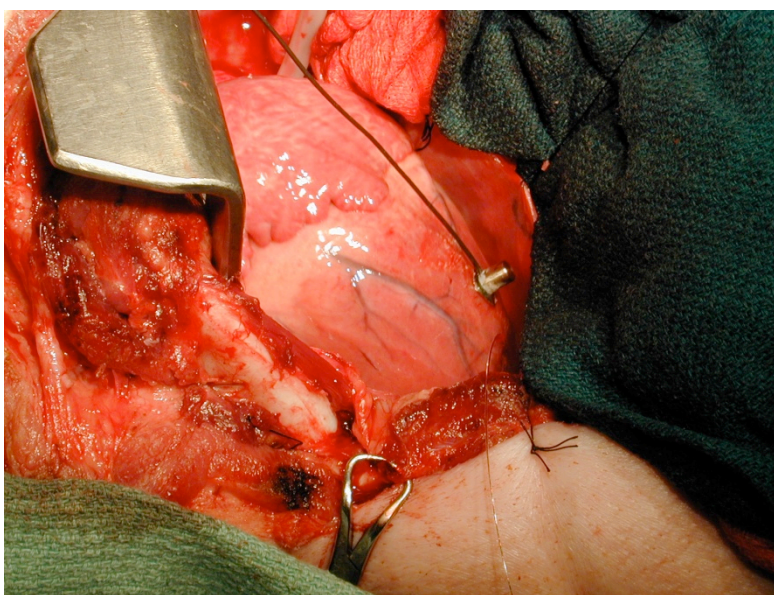

Figure 4 : example of open chest surgery in one animal and accelerometer position on the epicardium surface of the heart.

The measured signals were firstly amplified (Millar Instruments,TCB-600 ; Bruel Kjaer, 2635) and digitized by using a data acquisition system (Axoscope). The signals were recorded under four different cardiac inotropic conditions: baseline condition, ischemia, increased LV afterload by mechanical constriction of the aorta and decreased afterload by injection of sodium nitroprussiate. The myocardial ischemia was caused by the

mechanical obstruction of blood flow in the left descending coronary artery. The acquisition protocol was designed to obtain signals that can be relevant for different studies. In this paper, attention is only focussed on the intra-ventricular pressures.

Identification of the model parameters

Identification algorithm

The objective of the parameter identification is to minimize an error function defined as the difference between the experimental and the simulated ventricular pressure. The synthesized pressure is obtained by simulating the proposed model with a specific set of parameter values *P*, which is composed of the time of electrical activation, the activation duration and the maximum level of *EMDF*, for the septum, lateral, anterior and inferior walls. These parameter values are assumed to be the same for the three anterior segments and the three inferior segments. Thus, 9 parameters values must be identified and *P* is defined as *P*=[*T_ septum*, *T_ ant_inf*, *T_lat*, *K_ septum*, *K_ ant_inf*, *K_lat*, *RDP_ septum*, *RDP_ ant_inf*, *RDP_lat*]

The error function used to determine the optimal set of parameters *P** among all the possible *P* is defined as the sum of the absolute values of the difference between experimental data and simulation, calculated for the whole cardiac cycle:

$$\varepsilon = \sum_{t=\tau_{QRS_i}}^{\tau_{QRS_{i+1}}} \left| \Pr essure_{simulated}(t) - \Pr essure_{real}(t) \right|$$

where $t = \left[\tau_{QRS_i}, ..., \tau_{QRS_{i+1}} \right]$ and τ_{QRS_i} represents the QRS detection instant for beat *i*.

Evolutionary Algorithms (EA) have been chosen because they are particularly adapted to this optimization problem. In fact, the error function is not differentiable and it is necessary to use an algorithm that does not require to compute the derivative of the error. In addition, EA can be employed to find an optimal configuration for a given system within specific constraints because of their generic definition.

EA are stochastic search methods inspired from the natural selection process. Each "individual" of a "population" is characterized by a set of parameters (or

"chromosomes"). In these algorithms, the set of parameters *P* characterizes each "individual" of a "population". In order to reduce the search space, parameter values were bounded to the physiologically plausible intervals: [300 900] for the activation duration (ms), [5 9] for the maximum level of *EMDF* (µM) and [1 150] for the electrical activation instants (ms). These intervals have been defined from physiological knowledge of cardiac behavior.

An initial population is created, usually from a set of random "chromosomes". The parameter values of a given individual are independently generated from a uniform distribution defined under the corresponding feasibility interval. This population will "evolve", improving its global performance, by means of an iterative process. Each iteration of an EA involves a competitive selection, by means of the "fitness" function. Solutions with high "fitness" values are recombined with other solutions (cross-over) and small, random modifications of a chromosome can also be introduced (mutation). Explicitly, once the error function has been evaluated for each individual, selection is carried out by means of the "Roulette Wheel" method, adapted for function minimization, in which the probability of selecting a given individual depends on the value of its error function, divided by the sum of all the error values of the population. Only standard genetic operators, defined for real-valued "chromosomes", have been used in this work: "uniform crossover", which creates two new individuals (offspring) from two existing individuals (parents), by randomly copying each "allele" (i.e., parameter value) from one parent or the other, depending on a uniform random variable; and "Gaussian mutation", which creates a new individual by randomly changing the value of one allele (selected randomly), based on a Gaussian distribution around the current value.

The convergence and robustness properties of EA depend upon adequate individual coding, proper definition of the fitness function and selection of appropriate genetic operators for crossover and mutation. The mutation operators help the EA process to explore the search space and prevent convergence to a local minimum. More details on EA can be found on (Michalewicz 1994).

Robustness analysis

In order to test the robustness of the identification method, the algorithm was repeated five times on the ventricular pressure signal of the first pig. Figure 5 shows boxplots of the 9 identified parameters: activation duration [*T_ septum*, *T_ ant_inf*, *T_lat*], maximum level of *EMDF* [*K_ septum*, *K_ ant_inf*, *K_lat*], and *RDP* periods [*RDP_ septum*, *RDP_ ant_inf*, *RDP_lat*].
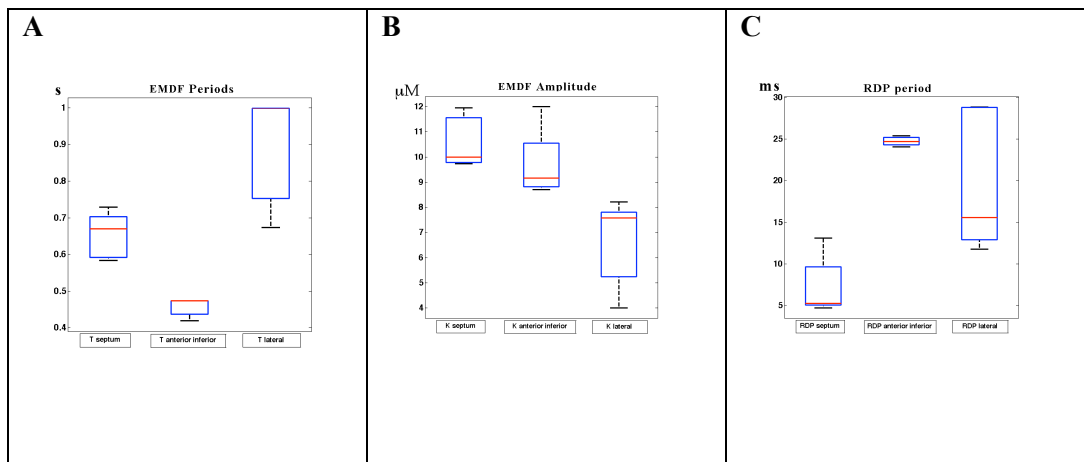
Figure 5: Boxplot of the ten identified parameters for the pig : A) *EMDF* periods [*T_ septum*, *T_ ant_inf*, *T_lat*], B) *EMDF* amplitudes [*K_ septum*, *K_ ant_inf*, *K_lat*], and C) *RDP* periods [*RDP_ septum*, *RDP_ ant_inf*, *RDP_lat*].

Parameters dispersion for the five identification processes can be observed in Figure 5, for the septum, the lateral and anterior walls. The parameters corresponding to the lateral wall are characterized by the highest dispersions. This observation is particularly true for the *RDP* parameter, which has less influence on ventricular pressure.

Results and Discussion

Global Hemodynamics

Figure 6 presents the simulation of global hemodynamic variables: ventricular pressure, flow and volume. The simulation is based on parameter values from the literature: *i)* cellular automata parameters were adjusted to fit electrical activation times from (Durrer

et al. 1970), *ii)* the activation duration was set to 400ms (Bovendeerd, Borsje et al. 2006) and *iii)* the maximum level of *EMDF* is fixed at 7 μM (Kerckhoffs, Bovendeerd et al. 2003).
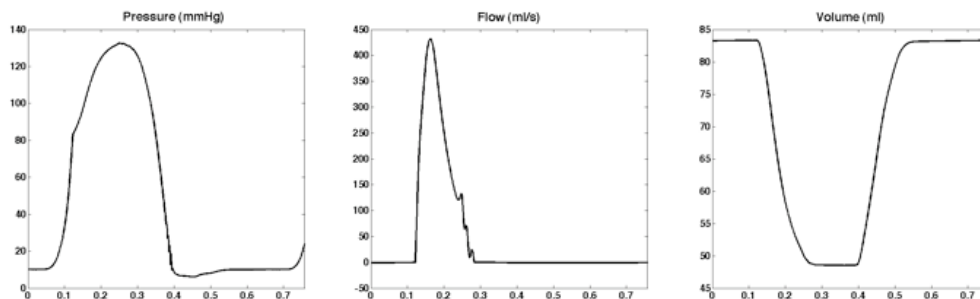

Figure 6: Model simulation of ventricular hemodynamic variables for one beat: intra-ventricular pressure (mmHg), aortic flow (ml/s) and ventricular volume (ml).

The global shapes of the generated pressure and flow signals appear realistic when compared with real data or those simulated from similar models (Kerckhoffs, Bovendeerd et al. 2003). The variation of ventricular volume reflects the pumping action of the cardiac model, and the pressure-volume curve is characteristic of the change of cardiac stiffness during the cardiac cycle.
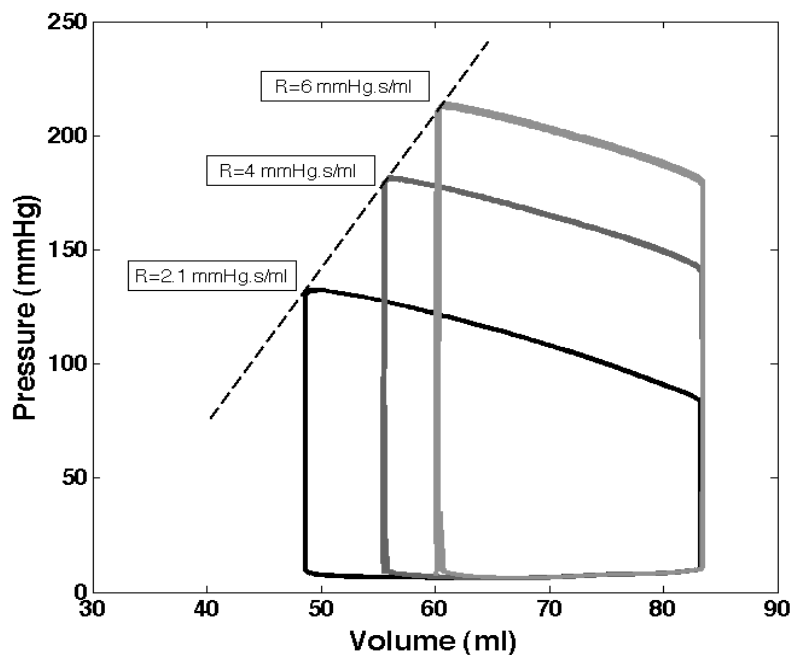
Figure 7: Simulation of the left ventricular pressure and volume (PV loop) with increased afterload resistance (R) leading to a rise in ventricular pressure. The linearity of the end-systolic pressure that is characteristic of the ventricular behaviour

Some parameter values can be varied to test the behaviour of the model. For example, Figure 7 shows that a rise of the output resistance leads to a rise in ventricular pressure. The afterload resistance is respectively equal to R=2.1 mmHg.s/ml, R=4 mmHg.s/ml and R=6 mmHg.s/ml for the first, second and third *in silico* experiments. This reaction is physiologically realistic because, in these conditions, the ventricle must develop a higher pressure to eject the blood in the aorta. The pressure-volume loop obtained with different resistances is shown in Figure 7, which illustrates the linearity of the end-systolic pressure characteristic of the ventricular behaviour

Ventricular pressure

The identification approach is applied to the intra-ventricular pressures of the 3 pigs. The experimental and simulated pressure signals are compared in the error function, which

has to be minimized using EA as described before. All the identified parameters are summarized in the table of APPENDIX C.
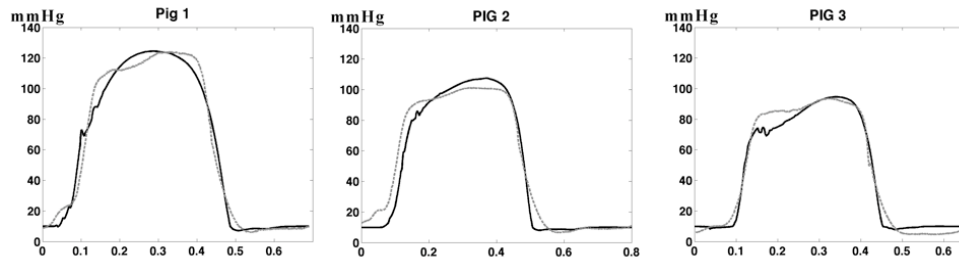

Figure 8 : Comparison between simulated pressure (black line) and experimental pressure (grey line) for the three pigs in stationnary conditions.

Figure 8 presents the simulated and experimental pressures for the three pigs in steady-state. The range of systolic pressure values is coherent with published values. But, it can also be noticed that these curves have particular wave shapes and durations. This observation is particularly visible during the systole (top of the curve). In fact, the rebound of the ventricular pressure, which can be remarked, is characteristic of the asynchronous activation of myocardium during cardiac contraction.

The good adaptation of the model to experimental data can be observed and the global morphology of the curve is reproduced. In fact, the ventricular pressure is a variable that reflects the macroscopic cardiac behavior. The pressure signal is the result of the combination of different segments activity. It depends mainly on the electrical propagation and the association of the different electrical activation dynamics. So, even if the *EMDF* profile is basic, the combination of the segments variables brings a realistic pressure profile.

For the steady-state conditions, the electrical activation times (T_{EA}) can be compared for the three pigs. The Bull's eye representation is used to present the fitted parameter values for the twelve myocardial segments. The Bull's eye diagram allows the description of the myocardial segments (Figure 9); the parameters can be easily interpreted because they can be compared to available data (Durrer, van Dam et al. 1970). The maximum T_{EA} reaches, respectively, 96.5 ms, 139.3 ms, and 131.5 ms for the first, second, and third pig.

These times are particularly high for the three pigs. By comparison, the work described in (Durrer, van Dam et al. 1970) reports that the maximum electrical activation time is normally about 65 ms in human adults.
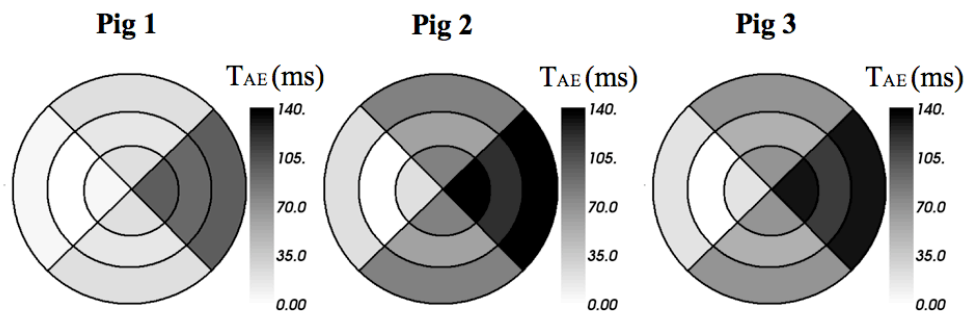

Figure 9: Electrical action times (T_{EA}) for the three pigs (ms). The maximum T_{EA} is equal to 96.5 ms, 139.3 ms and 131.5 ms, respectively, for the first, second and third pig.

The pressure morphology is well reproduced, mainly because the model integrates a regional description of the myocardial behavior. Thus, these results show the appropriateness of the proposed model that both gives realistic simulations and explains the particularities of some ventricular pressures, facilitating the interpretation of experimental data.

Afterload variations

Figure 10 shows the 3 curves obtained after the identification for different afterload conditions. The first observation is the model's ability to reproduce experimental data. Some well-known physiological phenomena are reproduced, like the rise of ventricular pressure with afterload.

It is interesting to note the model adaptation to different experimental curves. The ventricular pressure profile is well reproduced, especially concerning the curve duration and the particular morphology of signals from each pig. Moreover, some discontinuities can be observed on some curves, for example, for the curve corresponding to afterload 1. These can be explained by the asynchronous activation of the different segments of the model, and the spatial resolution of the model.
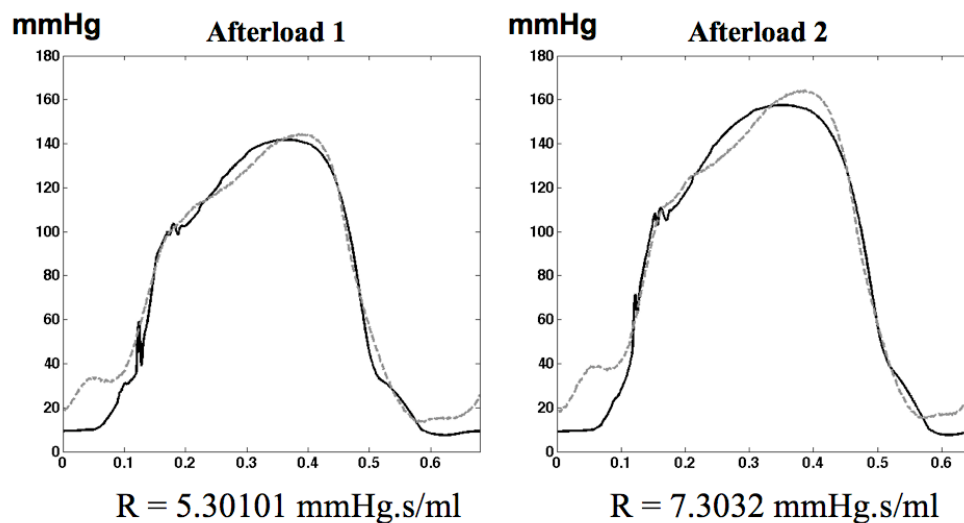
Figure 10: Comparison between simulated pressure (black line) and experimental pressure (grey line) for the first pig with two afterload conditions. The afterload resistances, which have been identified, are coherent with the afterload increase.

The identification returns the estimated afterload resistance values. For the afterloads 1 and 2, the resistance value is, respectively, equal to 5.30101 mmHg.s/ml and 7.3032 mmHg.s/ml. These parameter values are coherent with the systolic pressure rise, which increases with the afterload

Model limitations

Although the results obtained for this application are encouraging, the proposed model includes some limitations, due to the simplifying assumptions on the electro-mechanical coupling and the absence of a direct mechanical coupling between segments. The main consequence of the latter point is the inability of the model to reproduce ventricular torsion.

Concerning the electro-mechanical coupling, it is clear that an analytic profile is not accurate enough to describe the complexity of calcium dynamics and this can have an influence on the macroscopic behavior. Although the use of such analytical driving

functions to represent the mean tissue-level calcium dynamics has been previously employed in different models, to our knowledge, there is no experimental data to validate or improve this kind of representation. However, it should be possible to simulate these mean values by aggregating a set of coupled cellular-level models accounting for intra and extracellular calcium dynamics, such as the one presented in (ten Tusscher, Noble et al. 2004). This is one of the future directions intended for our work.

Conclusion

The present paper proposes a new multiformalism electromechanical model of the left ventricle. An identification algorithm is used to define the model parameters as functions of experimental ventricular pressures. The simulations, obtained after adjustment of the parameters, show that the model effectively reproduces ventricular pressure curves. The model accuracy is mainly due to its structure, which takes into account a simplified geometry, a description of the electrical, mechanical, and hydraulic activities, a physiological segmentation and the possibility of representing the asynchronous electro-mechanical activation of different ventricular segments.

One of the advantages of the approach is the low computational cost, which facilitates parameter identification. In fact, the simulation of one cardiac cycle (800 ms of simulation), takes about 20s on a dual-core Intel Xeon 2.66Ghz; whereas a complete electro-mechanical model based on Finite Element (Nickerson, Smith et al. 2005) can take three weeks on an IBM Regatta P690 high-performance computer for 1000 ms of simulation.

Although the main objective of this study is to show the similarities between simulated and experimental intra-ventricular pressure waveforms, the identified electro-mechanical parameters have also been analyzed. The robustness of the identification has been tested by applying the identification algorithm 5 times on the same dataset.

The important point of this work is the validation of the model to reproduce realistic ventricular pressure. These preliminary results are encouraging for the application of the

model to non-invasive data such as arterial pressure or myocardial strain. Therefore, future work will focus on the validation of the modeling approach in a clinical context. Healthy and pathological cases could be studied to test the model-based approach for interpretation. Such an evaluation of the proposed model-based method should allow the development of new diagnostic applications to heart failure and planning assistance for cardiac resynchronization therapy.

Acknowledgments

APPENDIX A: The Bond Graph Formalism

The Bond Graph (BG) formalism is a diagram-based method that is particularly powerful for representation of multi-energy systems, since it is based on the representation of power exchanges; the terminology, the rules, and the construction of Bond Graph models are the same for all energy domains. For example, in the mechanical domain, the effort variable e is the force and the flow variable f is the rate; whereas, in the hydraulic domain, the effort variable e is the pressure and the flow variable f represents flow. The power is the product of the effort and the flow: $P=e.f$. The elements of the Bond Graph language can be classified as:

Passive elements: R, C and I

- Resistive element (R):

    The resistive element R is used to describe dissipative phenomena and can represent electrical resistors, dashpots or plugs in fluid lines.

- Capacitive element (C):

    The capacitive element C is used to describe energy storage and can represent springs or electrical capacitors.

- Inertial element (I):

The inertial element I is used to model inductance effects in electrical systems and mass or inertia effects in mechanical or fluid systems.

Active elements: Se and Sf

An effort source is an element that produces an effort independently of the flow, and a flow source an element that produces flow independently of the effort.

Junction elements: 0, 1, TF, GY

- 0 junction:

  The 0 junction is characterized by the equality of the efforts on all its links, while the corresponding flows sum up to zero, if power orientations are taken positive toward the junction.

- 1 junction:

  1 junction is characterized by the equality of the flows on all its links, and the corresponding efforts sum up to zero with the same power orientations.

- Transformer (TF):

  The transformer TF conserves power and transmits the factors of power with scaling defined by the transformer modulus. It can represent an ideal electrical transformer or a mass-less lever.

- Gyrator (GY):

  A gyrator establishes a relationship between flow to effort and effort to flow and conserves power. It can represent a mechanical gyroscope or an electrical dc motor.

The Bond Graph formalism can be particularly useful for modelling physiological systems which often include various energy domains. For example, models of the vascular system (LeFèvre 1999; Diaz-Zuccarini 2003) are especially interesting since they take into account different energy phenomena (hydraulic, mechanic, chemical…).

APPENDIX B: Parameter Values

Some model Parameters values are not determined by the identification algorithm. They are taken from the literature.

	Parameter values	*Source*
Preload		
Se	10 mmHg	Estimated
Afterload		
C	0.219 ml/mmHg	(Ursino and Magosso 2000)
R	2.1 mmHg.s/ml	(Ursino and Magosso 2000)
I	0.00082 mmHg.s2/ml	(Ursino and Magosso 2000)
Valve		
Rpass	0.01 mmHg.s/ml	Estimated
Rblo	100 mmHg.s/ml	Estimated
Ventricle		
Valvular Plan		
C	0.05 ml/mmHg	Estimated
Hydraulic Resistance		
T1	0.03 s	Estimated
T2	0.05*RR s	Estimated
Inertance		
I	0.0001 mmHg.s2/ml	Estimated
Geometric Parameters		
Mean fibre angle	$\pi/12$	(Streeter 1979)
Thickness	1 cm	(Streeter 1979)
Active Capacity		
Tref	125 kPa	(Hunter 1995)
β	1.45	(Hunter 1995)
n_ref	4.25	(Hunter 1995)
pC50_ref	5.33	(Hunter 1995)
B2	0.31	(Hunter 1995)
Passive Capacity		
C1	15.188 kPa	(Humphrey, Strumpf et al. 1990; Chaudhry 1996)
C2	73.432 kPa	(Humphrey, Strumpf et al. 1990; Chaudhry 1996)
C3	1.4016 kPa	(Humphrey, Strumpf et al. 1990; Chaudhry 1996)
C4	-19.482 kPa	(Humphrey, Strumpf et al. 1990; Chaudhry 1996)
C5	18.887 kPa	(Humphrey, Strumpf et al. 1990; Chaudhry 1996)

APPENDIX C: Identified Parameter Values

	Pig 1			Pig 2	Pig 3
	stationary	*Postload 1*	*Postload 2*	*stationary*	*stationary*
K septum	11.9 μM	10.5 μM	9.1 μM	11.7 μM	12 μM
K anterior inferior	9.1 μM	9.4 μM	9.2 μM	11.6 μM	10.8 μM
K lateral	7.5 μM	6.7 μM	6.5 μM	4 μM	5.6 μM
T septum	583.9 ms	491 ms	502 ms	604.8 ms	833.1ms
T anterior inferior	473.7 ms	545.6 ms	552.1 ms	436.1 ms	390.8 ms
T lateral	998 ms	910.3 ms	809.1 ms	998.7 ms	864.2 ms
UAP septum	5.24 ms	16.5 ms	14.8 ms	19.7221 ms	17.2 ms
UAP anterior inferior	25.17 ms	38.2 ms	24.2 ms	20.1468 ms	20.8 ms
UAP lateral	15.57 ms	34.5 ms	30.7 ms	23.2628 ms	27.4 ms
Postload Resistance		5.3 mmHg.s/ml	7.3 mmHg.s/ml		

References

Guarini, M., J. Urzua, A. Cipriano and W. Gonzalez (1998). "Estimation of cardiac function from computer analysis of the arterial pressure waveform." IEEE Trans Biomed Eng 45(12): 1420-8.

Palladino, J. L. and A. Noordergraaf (2002). "A paradigm for quantifying ventricular contraction." Cell Mol Biol Lett 7(2): 331-5.

Luo, C. H. and Y. Rudy (1994). "A dynamic model of the cardiac ventricular action potential. II. Afterdepolarizations, triggered activity, and potentiation." Circ Res 74(6): 1097-113.

ten Tusscher, K. H., D. Noble, P. J. Noble and A. V. Panfilov (2004). "A model for human ventricular tissue." Am J Physiol Heart Circ Physiol 286(4): H1573-89.

Wong, A. Y. (1973). "Myocardial mechanics: application of sliding-filament theory to isovolumic concentration of the left ventricle." J Biomech 6(5): 565-81.

Hunter, P. J. (1995). "Myocardial constitutive laws for continuum mechanics models of the heart." Adv Exp Med Biol 382: 303-18.

Rice, J. J., M. S. Jafri and R. L. Winslow (2000). "Modeling short-term interval-force relations in cardiac muscle." Am J Physiol Heart Circ Physiol 278(3): H913-31.

Kerckhoffs, R. C., P. H. Bovendeerd, J. C. Kotte, F. W. Prinzen, K. Smits and T. Arts (2003). "Homogeneity of cardiac contraction despite physiological asynchrony of depolarization: a model study." Ann Biomed Eng 31(5): 536-47.

Chaudhry, H. R. B., B.; Findley T. (1996). "Stresses and Strains in the Passive Left Ventricle." Journal of Biological Systems 4: 535-554.

Nash, M. (1998). Mechanics and Material Properties of the Heart using an Anatomically Accurate Mathematical Model. Auckland.

Kerckhoffs, R. C., O. P. Faris, P. H. Bovendeerd, F. W. Prinzen, K. Smits, E. R. McVeigh and T. Arts (2003). "Timing of depolarization and contraction in the paced canine left ventricle: model and experiment." J Cardiovasc Electrophysiol 14(10 Suppl): S188-95.

Verdonck, P. R., Vierendeels J.A. (2002). "Fluid-Structure Interaction Modelling of Left Ventricular Filling." International Conference on Computational Science 275 – 284.

Kerckhoffs, R. C., M. L. Neal, Q. Gu, J. B. Bassingthwaighte, J. H. Omens and A. D. McCulloch (2007). "Coupling of a 3D finite element model of cardiac ventricular mechanics to lumped systems models of the systemic and pulmonic circulation." Ann Biomed Eng 35(1): 1-18.

Nickerson, D., N. Smith and P. Hunter (2005). "New developments in a strongly coupled cardiac electromechanical model." Europace 7 Suppl 2: 118-27.

Hirabayashi, S., M. Inagaki and T. Hisada (2008). "Effects of Wall Stress on the Dynamics of Ventricular Fibrillation: A Simulation Study Using a Dynamic Mechanoelectric Model of Ventricular Tissue." J Cardiovasc Electrophysiol.

Shim, E. B., H. M. Jun, C. H. Leem, S. Matusuoka and A. Noma (2008). "A new integrated method for analyzing heart mechanics using a cell-hemodynamics-autonomic nerve control coupled model of the cardiovascular system." Prog Biophys Mol Biol 96(1-3): 44-59.

Le Rolle, V., A. I. Hernandez, P. Y. Richard, J. Buisson and G. Carrault (2005). "A bond graph model of the cardiovascular system." Acta Biotheoretica 53: 295-312.

Le Rolle, V., A. I. Hernández, P.-Y. Richard and G. Carrault (2008). "An autonomic nervous system model applied to the analysis of orthostatic tests." Modelling and Simulation in Engineering In press.

Bardou, A. L., P. M. Auger, P. J. Birkui and J. L. Chasse (1996). "Modeling of cardiac electrophysiological mechanisms: from action potential genesis to its propagation in myocardium." Crit Rev Biomed Eng 24(2-3): 141-221.

LeFèvre, J. L., L. and Couteiro B. (1999). "A bond graph model of chemo-mechanical transduction in the mammalian left ventricle." Simulation Practice and Theory 7: 531-552.

Hernandez, A. I. (2000). Fusion de signaux et de modèles pour la caractérisation d'arythmies cardiaques. Rennes.

Hernandez, A. I., G. Carrault, F. Mora and A. Bardou (2002). "Model-based interpretation of cardiac beats by evolutionary algorithms: signal and model interaction." Artif Intell Med 26(3): 211-35.

Diaz-Zuccarini, V. A. (2003). Etude des conditions d'efficacité du ventricule gauche par optimisation téléonomique d'un model de son fonctionnement. Lille.

Silva, C. E., L. D. Ferreira, L. B. Peixoto, C. G. Monaco, M. A. Gil and J. Ortiz (2002). "Study of the myocardial contraction and relaxation velocities through Doppler tissue imaging echocardiography: A new alternative in the assessment of the segmental ventricular function." Arq Bras Cardiol 78(2): 200-11.

Bovendeerd, P. H., P. Borsje, T. Arts and F. N. van De Vosse (2006). "Dependence of intramyocardial pressure and coronary flow on ventricular loading and contractility: a model study." Ann Biomed Eng 34(12): 1833-45.

Taber, L. A., M. Yang and W. W. Podszus (1996). "Mechanics of ventricular torsion." J Biomech 29(6): 745-52.

Humphrey, J. D., R. K. Strumpf and F. C. Yin (1990). "Determination of a constitutive relation for passive myocardium: II. Parameter estimation." J Biomech Eng 112(3): 340-6.

Back, L. (1977). "Left ventricular wall and fluid dynamics of cardiac contraction." Math. Biosci 36: 257 -297.

Ursino, M. and E. Magosso (2000). "Acute cardiovascular response to isocapnic hypoxia. I. A mathematical model." Am J Physiol Heart Circ Physiol 279(1): H149-65.

Michalewicz (1994). Genetic Algotithms + Data Structures = Evolution Programs. New York, Springer-Verlag.

Durrer, D., R. T. van Dam, G. E. Freud, M. J. Janse, F. L. Meijler and R. C. Arzbaecher (1970). "Total excitation of the isolated human heart." Circulation 41(6): 899-912.

Streeter, D. D. (1979). Gross morphology and fiber geometry in the Heart, in Handbook of Physiology Volume 1: the Cardiovascular System.